NUCL SCI TECH (2021) 32:12
https://doi.org/10.1007/s41365-021-00848-4

Cage-like radiotherapy system for noncoplanar radiotherapy

Chuan-Meng Niu[1] · Ming-Hui Li[1] · Jian-Rong Dai[1]

Received: 17 August 2020 / Revised: 12 November 2020 / Accepted: 16 November 2020 / Published online: 10 February 2021

Abstract The aim of this study was to design a cage-like radiotherapy system (CRTS) to further promote the clinical application of noncoplanar radiotherapy. The CRTS comprises two stands, two O-rings, several arc girders, an X-ray head, an imaging subsystem, and a treatment couch. The X-ray head rotates with O-rings around the patient's body and slides along the arc girder. Compared with the C-arm linear accelerator (C-Linac), the clinically available spatial irradiation angle ranges (SIARs) of the CRTS for the head, chest, and abdomen were 33%, 63.6%, and 62.6% larger, respectively. Moreover, according to a preliminary planning comparison based on the dose distribution simulation method, the CRTS achieved much better protection of normal tissue than the C-Linac. Furthermore, the CRTS enabled accurate noncoplanar irradiation without movement of the body being irradiated, allowed automatic control of the movements of different parts without risk of collisions, and provided continuous radiation over an angle that considerably exceeded a full turn. These advantages make CRTS very promising for noncoplanar radiotherapy.

Keywords Radiotherapy system · Noncoplanar radiotherapy · Spatial irradiation angle range · Spherical surface area

1 Introduction

In principle, noncoplanar beam geometry is a superset of the coplanar beam solution space. It has been shown to yield superior dosimetry when it is appropriately implemented [1–4]. Some noncoplanar static beams or arcs have demonstrated substantial dosimetric advantages over current static intensity-modulated radiation therapy and volumetric-modulated arc therapy, which employ only coplanar beams or arcs. These advantages of noncoplanar static beams or arcs include improved dose conformality, normal-organ sparing, and dose escalation for treatments to the brain [5, 6], head and neck [7, 8], liver [1], lung [9], breast [10], and prostate [11–13]. However, clinical use of noncoplanar beams or arcs in external radiation therapy has been limited, with the exception of specialized stereotactic radiosurgery machines, such as the Gamma Knife, Cyber Knife, and conventional linear-accelerator-based stereotactic radiosurgery using cone collimators and multiple intersecting arcs. Adoption of noncoplanar radiotherapy on the most widely available C-arm gantry systems has been hindered by technical challenges, including the lack of practical integrated beam orientation and fluence optimization tools, as well as collision hazards and long treatment times. Nevertheless, steady progress has been made in noncoplanar treatment planning and delivery research in recent years. Several researchers have examined automated techniques for determining the optimal configuration of noncoplanar beams [14]. A robust

This work was supported by the National Natural Science Foundation of China (No. 11475261) and partially supported by the National Key Project of Research and Development of China (No. 2016YFC0904600).

✉ Jian-Rong Dai
dai_jianrong@163.com

[1] Department of Radiation Oncology, National Cancer Center / National Clinical Research Center for Cancer/ Cancer Hospital, Chinese Academy of Medical Sciences and Peking Union Medical College, Beijing 100021, China

commercial solution that optimizes the beam angle selection for noncoplanar intensity-modulated radiation therapy or volumetric modulated arc therapy will likely be developed in the near future. Collisions can be prevented with pretreatment 3D modeling and the use of proximity sensors [15–18]. Many newer C-arm linear accelerators (C-Linacs) equipped with a robotic couch and gantry are technically capable of automation, which enables effective plan delivery [11].

These recent developments have revitalized interest in noncoplanar planning. However, the C-Linac has the challenging issue of machine geometric limitations, which exclude many noncoplanar angles. Thus, the restricted noncoplanar angle selection range may inhibit achievement of optimal planning dosimetry. Moreover, when delivering noncoplanar beams and moving the treatment couch and gantry, great caution must be exercised to prevent potential setup errors. This is especially the case during treatment with a large number of noncoplanar beams [19, 20]. To overcome these problems and promote the clinical adoption of noncoplanar beams for external radiotherapy, we developed an innovative cage-like radiotherapy system (CRTS), for which a Chinese invention patent (application number: 2018100784318) is pending. This article describes the CRTS construction and the results of a preliminary comparative analysis with a C-Linac.

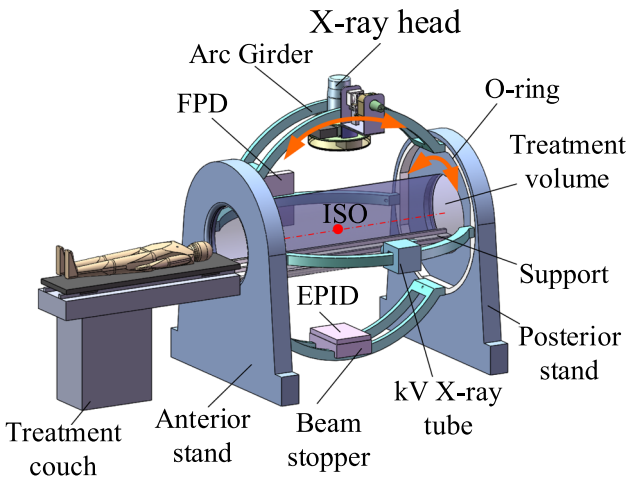

Fig. 1 (Color online) The CRTS has a cage-like structure. It mainly consists of two parallel stands, which provide high stability for the whole system, and several rotatable arc girders around the treatment volume, which carry the X-ray head and other ancillary equipment. FPD and ISO are the abbreviations of flat panel detectors and isocenter

2 Materials and methods

2.1 Introduction of the CRTS

The overall structure of the CRTS is presented in Fig. 1. Two stands are fixed to the ground in parallel, and their circular through-holes are located coaxially along the longitudinal axis. A free treatment volume is formed between the two stands. To prevent collisions, no moving elements are allowed to be present within this volume during the treatment process. A support board with three orthogonal translations is installed on the two stands by its two ends. The couch top can translate from the treatment couch to the support board and carry the patient to the irradiation position. One O-ring is embedded in each of the circular through-holes of the two stands. The gantry is mainly composed of several arc girders that stretch across the O-rings and rotate around the longitudinal axis that passes through the isocenter (ISO). The X-ray head, which includes an X-band accelerator and a multi-leaf collimator (MLC), is mounted on one of the arc girders and is moveable. The source-axis distance (SAD) remains fixed for the range of translation distances of the X-ray head along the arc girder. The X-ray head can be translated in two degrees of freedom: rotating around the treatment volume, and sliding on the arc girder along the longitudinal axis, thereby irradiating the body from different directions around the treatment volume.

The CRTS adopts a double-stand structure and has considerable overall support strength. Thus, multiple sets of slide rails or arc girders of the gantry can be installed between the two fixed stands to carry the imaging devices, counterweights, and other ancillary equipment, which facilitate the image-guided noncoplanar radiotherapy (Fig. 1). An electronic portal imaging device (EPID) and beam stopper are fixed together. They can translate synchronously with the X-ray head along the opposite arc girder. The beam stopper has two functions: blocking unwanted X-rays and providing a counterbalance.

To apply radiotherapy using the CRTS, the patient is first transported to the treatment position by the treatment couch top. Next, an imaging subsystem is used to identify any setup errors due to the support board motion. Then, the X-ray head is driven by the treatment plan to deliver the prescribed dose to the target area. It is not necessary to move the patient during the whole noncoplanar radiotherapy treatment process.

2.2 Design of overall structure

The basis of the overall structural design was to prevent a collision, which is the closest distance between the X-ray

head and the treatment volume. This distance cannot be less than the safety buffer distance, *s,* as shown in Fig. 2. This qualification can be expressed as the following inequality:

$$\left(H+\frac{D}{2}\right)\bullet\cos\alpha-\frac{d}{2}\bullet\sin\alpha-\frac{D}{2}\geq s, \tag{1}$$

where α indicates the maximum angle that the X-ray head can translate along the arc girder, and d denotes the diameter of the lower end of the X-ray head. The SAD can be calculated based on the schematic diagram shown in Fig. 2 using

$$\mathrm{SAD}=\frac{D}{2}+H+h, \tag{2}$$

where H indicates the distance between the lower surface of the X-ray head and the treatment volume surface when the X-ray head is at the neutral position, D denotes the diameter of the treatment volume, and h is the distance between the target and the lower surface of the X-ray head.

2.3 Design of the X-ray head

The X-ray head primarily consists of an X-band accelerator and an MLC, as shown in Fig. 3. No flattening filter is used, and a couple of Y jaws with the orthogonally arranged MLC work together to modulate the beam shape. The microwave subsystem is installed perpendicularly to the accelerator. A suitable SAD and a light weight can be obtained owing to the compact structure design of the X-ray head.

2.4 Computing method to calculate the spatial irradiation angle ranges (SIARs)

The X-ray source can ideally reach any positioning point on a virtual spherical surface that is centered at the ISO and has a radius equal to the SAD to be irradiated, which is known as 4π radiotherapy. However, the limitations of the mechanical structure mean that ideal 4π radiotherapy cannot be realized. The SIAR that is actually realized by the X-ray source is calculated using the following formula:

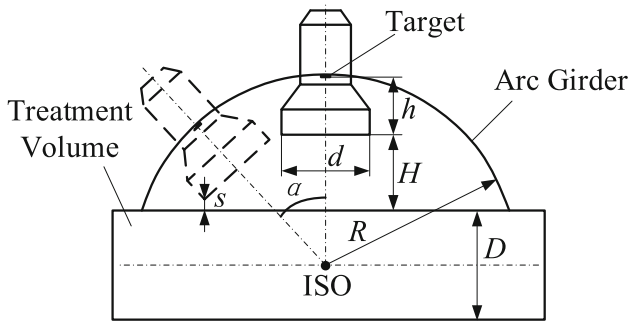

Fig. 2 The schematic diagram used to introduce the overall structure design basis

$$\varphi=\frac{S_\mathrm{r}}{S_\mathrm{s}}, \tag{3}$$

where φ represents the SIAR numerical value, S_r denotes the area of the partial spherical surface formed by the position points that the X-ray source can achieve, and S_s is the area of the entire virtual spherical surface, which is given by

$$S_\mathrm{s}=4\pi r^2, \tag{4}$$

where r is equal to the SAD.

2.5 SIAR of the CRTS

With the mechanical structure detailed in Sect. 2.1, the reachable spatial location points of the X-ray head of the CRTS form a drum-like spherical surface (similar to the whole spherical surface with two poles removed), which will not be changed, even for targets in different parts of the patient's body (Fig. 4). The drum-like spherical surface area ($^{\mathrm{c}}S_\mathrm{r}$) is readily obtained using SolidWorks evaluation tools (Premium 2014, Dassault Systems, France). The $^{\mathrm{c}}S_\mathrm{r}$ is entered into Eq. (3) to determine the SIAR of the CRTS.

2.6 SIAR of the C-Linac

The SIAR of the C-Linac is not a constant value; it varies widely depending on the patient body shape, tumor location, setup immobilization devices, and machine model [15]. To facilitate a comparison with the CRTS, we adopted an experimental method to measure the SIAR of the C-Linac. The measurements were performed on a Varian Edge Exact Couch combined with a Millennium MLC (Varian Medical Systems, TrueBeam Platform 2.5). The patient's presence was simulated by placing a cardiopulmonary resuscitation manikin (model GD/CPR10280; size 170 × 50 × 26 cm^3; Shanghai Chenbo Science and Education equipment factory) on the top of the couch. The SIARs of the C-Linac for treatments to the head, thorax, and abdomen were measured separately. The target locations of all three sites were assumed to be at the body center for which the widest SIAR could be accepted [17]. The target locations employed for the measurements are presented in Table 1. To determine the maximum gantry angle achievable for each couch position, the couch was rotated at 5° intervals, and the gantry was moved until the closest distance from the gantry to the couch or the manikin was 5 cm (Fig. 5). The couch angle was changed from 0° to 90° and from 270° to 360°.

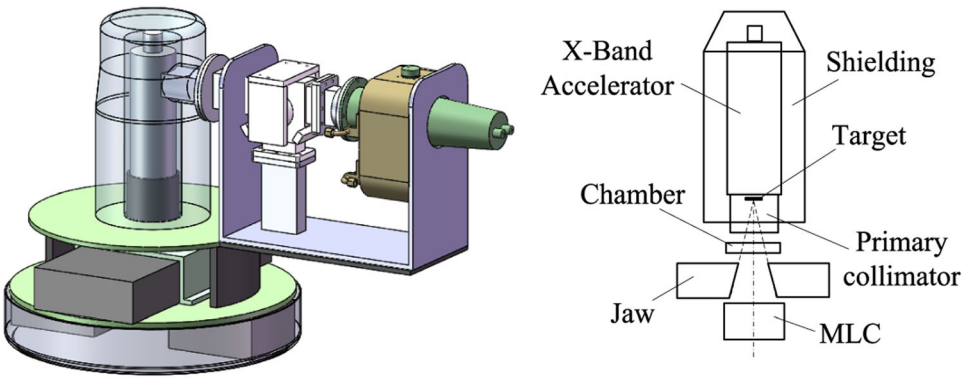

Fig. 3 (Color online) The X-ray head is mainly composed of an X-band accelerator (left) and a multileaf collimator (right)

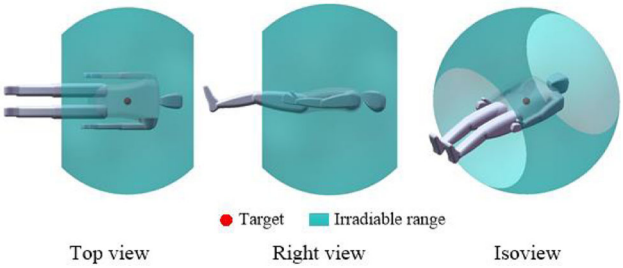

Fig. 4 (Color online) The spatial irradiation angle range of the cage-like radiotherapy system expressed as graphical images

Table 1 Target locations in the head, thorax, and abdomen

Tumor location	Vertical (cm)	Length (cm)	Lateral (cm)
Head	− 10	80	0
Thorax	− 10	116	0
Abdomen	− 10	140	0

Fig. 5 (Color online) Measurements of the spatial irradiation angle ranges of the C-arm linear accelerator (Edge) for treatment applied to the patient's head

2.7 Simulation method of the dose distributions

To simulate the CRTS dose distributions, a common C-Linac model was employed in the treatment planning system as a substitute for the CRTS. It was assumed to have the same SIAR. The beam angle of the CRTS could be determined by θ_1 and θ_2, where the longitudinal angle θ_1 is the rotation angle of the arc girder around the O-ring, and θ_2 is the rotation angle of the X-ray head along the arc girder (Fig. 6). The spatial geometric relationship yields

$$\theta_c = -\tan^{-1}\left(\frac{\tan\theta_2}{\sin\theta_1}\right), \tag{5}$$

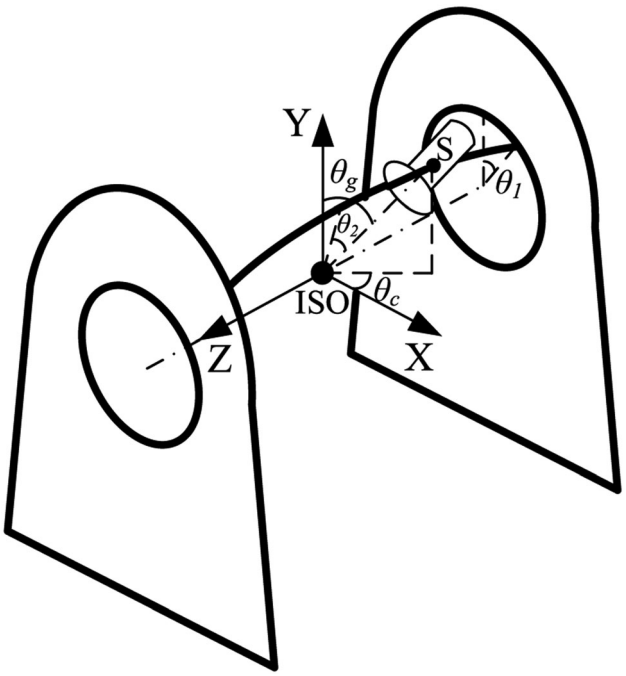

Fig. 6 The coordinate system *X*–*Y*-*Z* was built at the ISO. The *X*-axis is positive to the right, and the Y-axis is positive toward the upward position. The *Z*-axis is positive toward the anterior stand and is situated coaxially along the longitudinal axis

$$\theta_g = \cos^{-1}(\cos\theta_1 \bullet \cos\theta_2), \quad (6)$$

where θ_c and θ_g indicate the couch angle and the gantry angle, respectively, corresponding to the CRTS beam angle. The following formula can be derived from formulas (5) and (6):

$$\cos^2\theta_2 = \frac{\cos^2\theta_g \bullet \tan^2\theta_c + 1}{\tan^2\theta_c + 1}, \quad (7)$$

where θ_2 varies from $-\alpha$ to $+\alpha$. To simulate the CRTS dose distribution using the current treatment system, the beam angle should satisfy the following inequality:

$$\frac{\cos^2\alpha(1+\tan^2\theta_c) - 1}{\tan^2\theta_c} \le \cos^2\theta_g \le 1 \quad (8)$$

To verify the effectiveness of the simulation method of the CRTS dose distribution, Pinnacle version 9.10 (Koninklijke Philips N.V., Netherlands) was used to design the treatment plans for a breast patient case and a head patient case based on a beam angle selection map for the CRTS (Fig. 7) obtained by inequality (8). For the breast patient case, the prescribed dose was 48 Gy/6 fractions for the planning treatment volume (PTV). The dose limits for the organs at risk (OARs) are listed in Table 2. For the head patient case, the prescribed dose was 52.5 Gy/15 fractions for the planning treatment volume (PTV). The dose limits for the OARs are listed in Table 3.

For the breast plan based on the CRTS, two spatial arcs in the tangent plane of the breast along the longitudinal direction were selected to irradiate the target area, which we term the 'spatial volume modulated arc therapy (SVMAT)'. The first arc had a θ_1 of 34° and θ_2 ranged from − 45° to + 45°. The second arc had a θ_1 of 214° and θ_2 ranged from − 45° to + 45°. However, in the current

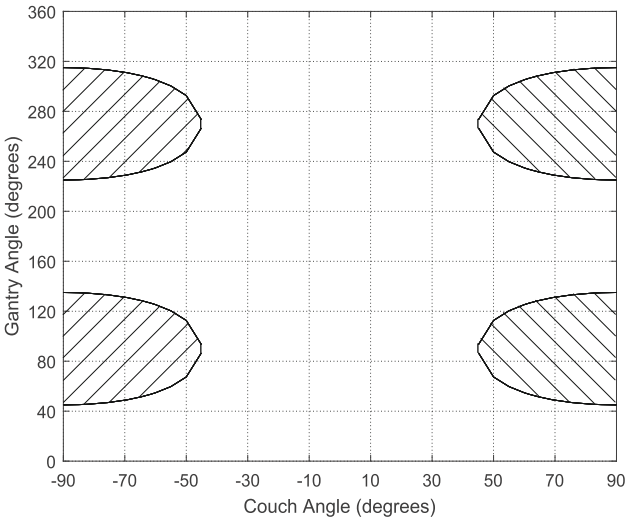

Fig. 7 The beam angle selection map for the CRTS. The zones filled with the oblique lines are the unreachable beam angle selection areas

Table 2 Normal tissue dose constraints for the breast patient

Structure	Index	Dose constraint
Contralateral breast	D_{mean}	< 4 Gy
Ipsilateral lung	D_{mean}	< 8 Gy
	$V_{20\%}$	< 10%
	$V_{5\%}$	< 20%
Heart	D_{mean}	< 2 Gy
Cord PRV	D_{max}	< 10 Gy

D_{mean}, mean dose; D_{max}, maximal dose; $V_{*\%}$, percentage of the volume receiving *% or more; PRV, planning organ at risk volume

Table 3 Normal tissue dose constraints for the head patient

Structure	Index	Dose Constraint
Spinal cord	D_{max}	< 30 Gy
Brain stem	D_{max}	< 30 Gy
Hippocampus	D_{mean}	< 30 Gy

version of Pinnacle, the available SVMAT trajectories were limited. Thus, we simulated SVMAT plans based on static multi-fields. Two sets of 19 control points were created by dividing θ_2 by a control spacing of 5°. Optimization was performed using 38 control points as 38 multi-field intensity-modulated radiotherapy (IMRT) plans. The internal adaptive convolution method and direct machine parameter optimization (DMPO) method of the planning system were selected for the dose calculation and optimization, respectively. The corresponding couch angle and gantry angle to each IMRT beam were calculated using Eqs. (5) and (6). We assumed that the simulated dose distribution was comparable with that of SVMAT. To make a preliminary comparison with the C-Linac, the common coplanar VMAT plan was designed using the same constraints as those of the SVMAT plan. Two partial coplanar arcs with gantry angles ranging from 35° to 220° were employed, and the control point spacing was set to 4°. The internal adaptive convolution method and SmartArc method were selected for the dose calculation and optimization, respectively. For the head SVMAT, five spatial arcs along the longitudinal direction were selected to irradiate the target area. For each arc, θ_1 was 90°, 120°, 150°, 180° and 210°, respectively, and θ_2 ranged from − 45° to + 45°. The head SVMAT plan was also simulated based on static multi-fields. The dose calculation method and optimization algorithm were selected to be the same as in the breast case. The noncoplanar VMAT (NVMAT) plan based on the C-Linac for the head case was also designed using the same constraints as the head SVMAT plan. Four

partial arcs were employed, and the control point spacing was set to 4°. For the first arc, the couch angle was 0° with a gantry angle ranging from 210° to 310°. For the second arc, the couch angle was 35° with a gantry angle ranging from 310° to 220°. For the third arc, the couch angle was 80° with a gantry angle ranging from 220° to 310°. For the fourth arc, the couch angle was 303° with a gantry angle ranging from 40° to 140°. The internal adaptive convolution method and SmartArc method were selected for the dose calculation and optimization, respectively.

3 Results

3.1 Major dimensions

For the distribution angle of the gamma knife radiation source in the latitudinal direction [21], α was proposed to be 45°. Considering the patient body shape, the preferred center bore diameter was set at 800 mm. The safety buffer distance, s, was set to 5 cm. The diameter of the lower end of the X-ray head, d, was designed to be 600 mm. According to inequality (1), the distance between the lower surface of the X-ray head at the neutral position and the treatment surface H should not be less than 536.4 mm. Owing to the compact structure design, the X-ray head was approximately 400 kg with a total height of 400 mm. The distance from the target to the lower surface of the X-ray head was designed to be 340 mm. By substituting the above parameters into Eq. (2), the SAD of the CRTS was approximately 1280 mm. The radius of the arc girder was designed to be 1300 mm, and the CRTS was approximately 4600 mm in length in the longitudinal direction (without a couch: 2600 mm), 3170 mm in height, and 2800 mm wide along the latitudinal direction.

3.2 Comparison of SIAR

The ${}^{c}S_r$ of the CRTS could be directly measured by Solidworks evaluation tools. The whole spherical area (S_s) could be calculated by Eq. (4) with a given SAD. By substituting the values of ${}^{c}S_r$ and S_s into Eq. (3), the SIAR of the CRTS was 2.83π. The reachable spatial location points of the X-ray head of the C-Linac formed different partial spherical surfaces for targets located in different body regions (Fig. 8). The surface areas of the head, thorax, and abdomen were measured using SolidWorks evaluation tools, and the SIARs of the C-Linac calculated by Eq. (3) were 2.72π, 1.73π, and 1.74π, respectively. Angling the beam toward the overhead area would greatly increase the low-dose region and is thus rarely employed in clinical applications.

After removing the bipolar region of the same size as that of the CRTS, the SIAR of the C-Linac for the patient's head was 2.13π (Table 4). The clinically available SIARs of the CRTS were 33%, 63.6%, and 62.6% larger than those of the C-Linac for the head and neck, chest, and abdomen, respectively. As reported in the literature [22–24], other radiotherapy systems, such as CyberKnife, Vero, and ZAP, also have smaller SIARs than the CRTS (Table 4). With respect to CyberKnife, its workspace is comprised of pre-assigned nodes that are roughly distributed on a half-sphere surface [22]. Considering that the C-Linac head can reach slightly lower than the couch level on the side, the maximum SIAR of CyberKnife is slightly larger than 2π and varies in accordance with the target location and the patient anatomy being treated. Meanwhile, Vero employs an O-ring instead of a C-arm to carry the Linac to rotate around the treatment couch. The O-ring can be skewed around its vertical axis. This skew provides a noncoplanar beam angle selection. The skew angle is limited to approximately ± 60° by mechanical interference between the couch and the O-ring [23]. The maximum SIAR of Vero is calculated to be approximately 2.67π using Eq. (3). However, Vero cannot eliminate the risk of collision owing to its overall structure being similar to that of the C-Linac. Moreover, its SIAR varies significantly in accordance with different target locations, especially for off-center targets. In terms of the Zap system, it is designed specifically for stereotactic radiosurgical (SRS) ablation of intracranial and head and neck lesions. It is mounted on a shielded treatment sphere with dual axes of independent rotation. Thus, the SIAR of ZAP is approximately 2π [24].

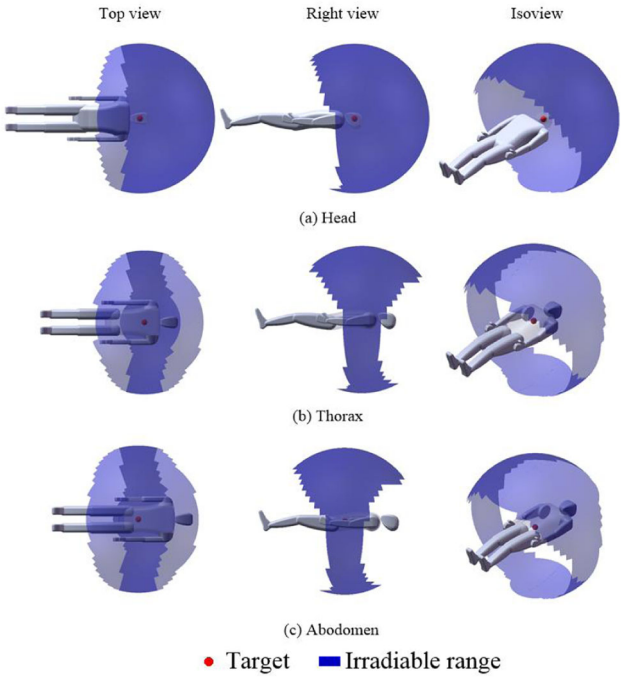

Fig. 8 (Color online) Spatial irradiation angle ranges of the C-arm linear accelerator expressed in graphic images

Table 4 SIARs of CRTS and C-Linac

Clinically available SIAR	CRTS	C-Linac (Edge, Varian)			CyberKnife [22]	Vero [23]	ZAP [24]
		Head	Thorax	Abdomen			
φ	2.83π	2.13π	1.73π	1.74π	2π	2.67π	2π

φ, numerical value of the spatial irradiation angle range

3.3 Dose distribution

Figure 9 shows the dose distributions of the breast SVMAT and VMAT for the breast patient. Table 5 summarizes the average dose volume indices for the targets and OARs. The two plans did not differ significantly in terms of any PTV evaluation (PTV_EVAL) parameters. However, the SVMAT plan for the CRTS significantly reduced the doses to the OARS. It is observed that the D_{mean} value of the contralateral breast is 95.9% lower for the SVMAT plan than for the VMAT plan. The D_{mean}, $V_{20\%}$, and $V_{5\%}$ values of the ipsilateral breast are, respectively, 57.6%, 25.9%, and 74.5% lower for the SVMAT plan than for the VMAT plan. The D_{mean} value of the heart is 93.6% lower for the SVMAT plan than for the VMAT plan. The D_{max} value of the planning OAR volume of the cord (PRV_Cord) is 90% lower for the SVMAT plan than for the VMAT plan.

Figure 10 presents the dose distributions of the SVMAT and NVMAT for the head patient. Table 6 summarizes the average dose volume indices for the targets and OARs. The SVMAT plan obtained better dose indexes of PTV than the NVMAT plan. The heterogeneity index (HI) of the SVMAT plan is 38.5% lower than that of the VMAT plan. Moreover, the SVMAT plan shows better OAR protection. The D_{max} values of the spinal cord, brain stem, and hippocampus are, respectively, 58.2%, 13.1%, and 15.3% lower for the SVMAT plan than for the NVMAT plan.

Table 5 Comparison of dosimetric parameters among SVMAT and VMAT for the breast patient

	Index	SVMAT	VMAT
PTV_EVAL	CI	0.91	0.93
	HI	0.087	0.065
	GI	2.98	2.41
Contralateral breast	D_{mean} (Gy)	0.06	1.45
Ipsilateral lung	D_{mean} (Gy)	1.78	4.22
	$V_{20\%}$ (%)	2.32	3.13
	$V_{5\%}$ (%)	6.22	24.36
Heart	D_{mean} (Gy)	0.17	2.67
PRV_ Cord	D_{max} (Gy)	0.21	2.12

CI, conformity index; HI, heterogeneity index; GI, gradient index

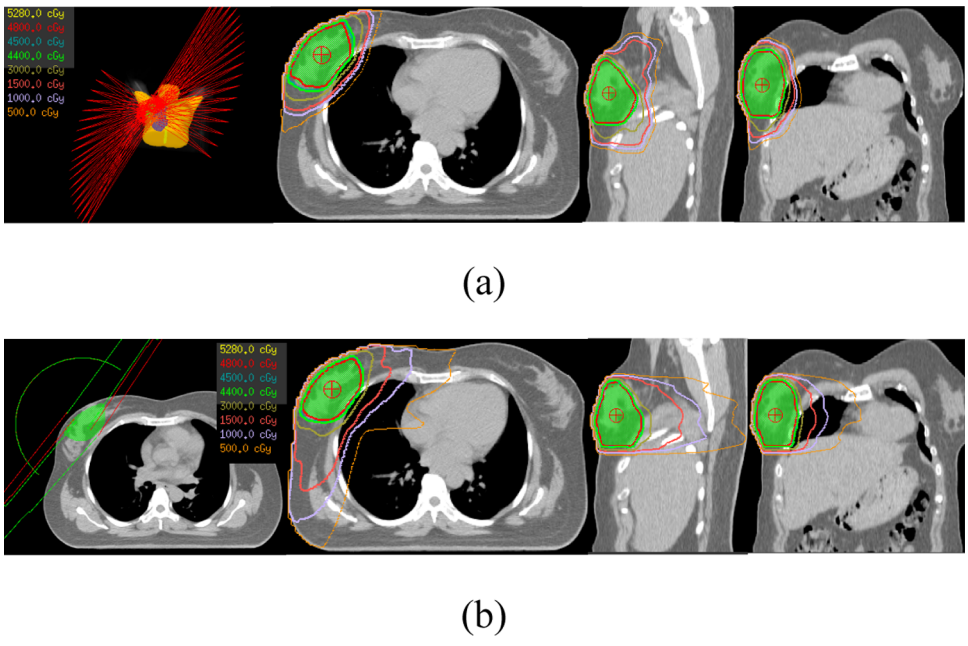

Fig. 9 (Color online) Beam arrangements and dose distributions for the breast patient: **a** SVMAT **b** VMAT

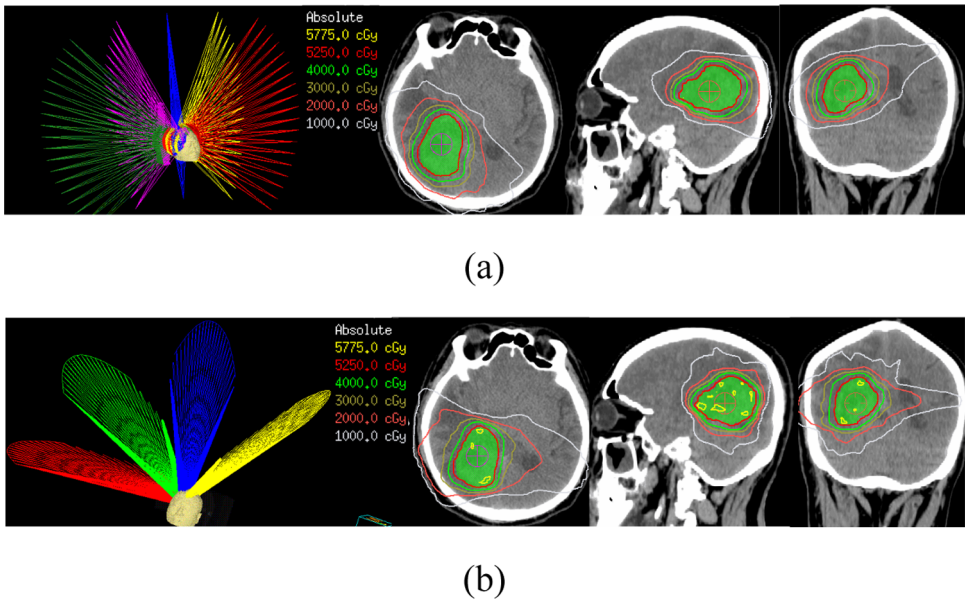

Fig. 10 (Color online) Beam arrangements and dose distributions for the head patient: **a** SVMAT **b** NVMAT

Table 6 Comparison of dosimetric parameters of SVMAT and NVMAT for the head patient

	Index	SVMAT	NVMAT
PTV_EVAL	CI	0.91	0.89
	HI	0.08	0.13
	GI	3.30	3.24
Spinal cord	D_{max} (Gy)	0.96	2.39
Brain stem	D_{max} (Gy)	13.78	15.86
Hippocampus	D_{max} (Gy)	39.73	46.9

4 Discussion

Compared with the C-Linac, the CRTS has several advantages for use in noncoplanar radiotherapy. First, the CRTS has a larger SIAR and a more uniform angle selection range than the C-Linac. Thus, the CRTS can be used to irradiate the patient from the anterior and posterior directions, as well as from the left and right directions, using the same beam angle selection range on a drum-like spherical surface (Fig. 4). In contrast, the available irradiation area using the C-Linac is very small when irradiating from the left, right, and posterior directions, but not from the anterior direction (Fig. 8). On account of this advantage, better OAR protection could be achieved for the breast and head patients using the CRTS than the C-Linac (Tables 5 and 6). Second, the CRTS enabled a more direct switch between two noncoplanar beams or arcs than the C-Linac. The CRTS X-ray head was directly translated from one noncoplanar radiotherapy position to another without moving the couch (Fig. 9a). In contrast, the C-Linac gantry could not be directly translated from the anterior noncoplanar angle to the posterior noncoplanar angle owing to the collision between the gantry and the couch (Fig. 11).

Using the C-Linac, the couch first had to be rotated to the non-collision area. Then, it was necessary to rotate the gantry to the posterior irradiation position. Finally, the couch had to be rotated to the noncoplanar position. These complex operations greatly increased the treatment time and collision risk for the C-Linac. Third, the CRTS enabled more convenient treatment planning than the C-Linac. The noncoplanar plan for the CRTS was directly designed without considering collision prevention. In contrast, it was difficult for the C-Linac to detect potential collisions during the treatment planning stage. A common method of collision prevention involves the use of a pretreatment simulation on a Linac. However, the discovery of a

Fig. 11 (Color online) Irradiation position switch between two noncoplanar beams for the C-arm linear accelerator

potential collision requires the treatment plan to be changed, which increases the noncoplanar planning time and difficulty [15]. Fourth, the CRTS provided much better assurance of patient positioning accuracy than the C-Linac. Fast treatment inherently enhances quality, as it becomes increasingly difficult for the patient to maintain the same position on the couch as the time required for treatment increases [16]. The CRTS enables noncoplanar treatment without the need for therapists to enter the treatment room. All treatment modalities can be performed quickly and are fully automated. Thus, the CRTS will markedly reduce the treatment time of noncoplanar radiotherapy and achieve a greater degree of treatment accuracy compared with the C-Linac.

In this article, the conceptual engineering design of the CRTS was described. However, our research remains in the preliminary stage; considerably more research should be conducted in future work. First, the mechanical design needs to be improved, including the detailed design of a compact X-ray head equipped with an MLC, design of the O-ring and slide girder structure, and design of an imaging subsystem. Second, the dosimetric benefits from the increased SIAR of the CRTS compared to other radiotherapy systems must be further studied. Based on the dose calculation methods and optimization algorithms to be developed for the SVMAT, many more patient cases could be enrolled for systematic research to demonstrate the dosimetric gains from employing a larger SIAR. Third, the shielding issues require further study. As the CRTS irradiates broader areas of the opposite wall and the ceiling of the therapy room than the C-Linac, additional costs would be incurred to augment the shielding, which is not necessary with conventional equipment. Fourth, the path algorithm for the CRTS should be further studied [25–27]. For noncoplanar treatment with multiple irradiation angles, the path algorithm should provide the optimal trajectory of the X-ray head to reach each irradiation position with the minimum distance. Accordingly, the maximum treatment efficiency can be realized.

5 Conclusion

In this article, we proposed the architecture of a novel CRTS that can realize noncoplanar radiotherapy by simply moving the X-ray head in two degrees of freedom without moving the treatment couch. The innovative mechanical design enables the CRTS to achieve a much larger SIAR than the C-Linac and produces no collision hazards. The present preliminary study of CRTS is expected to promote the clinical application of noncoplanar radiotherapy.

Acknowledgments The authors would like to thank Dong-Sheng Han, Wen Li, Yi-Xin Song, Yuan Tian, and Ke Zhang for their helpful discussions and assistance.

Author contributions All authors contributed to the study conception and design. Material preparation, data collection and analysis were performed by Chuan-Meng Niu, Ming-Hui Li and Jian-Rong Dai. The first draft of the manuscript was written by Chuan-Meng Niu and all authors commented on previous versions of the manuscript. All authors read and approved the final manuscript.

References

1. P. Dong, P. Lee, D. Ruan et al., 4π non-coplanar liver SBRT: a novel delivery technique. Int. J. Radiat. Oncol. Biol. Phys. **85**, 1360–1366 (2013). https://doi.org/10.1016/j.ijrobp.2012.09.028
2. D. Nguye, P. Dong, T. Long et al., Integral dose investigation of noncoplanar treatment beam geometries in radiotherapy. Med. Phy. **41**, 011905 (2014). https://doi.org/10.1118/1.4845055
3. K. Woods, D. Nguyen, A. Tran et al., Viability of Noncoplanar VMAT for liver SBRT compared with coplanar VMAT and beam orientation optimized 4π IMRT. Adv. Radiat. Oncol. **1**, 67–75 (2016). https://doi.org/10.1016/j.adro.2015.12.004
4. K. Nakagawa, Y. Aoki, M. Tago et al., Dynamic conical conformal radiotherapy using a C-arm-mounted accelerator: dose distribution and clinical application. Int. J. Radiat. Oncol. Biol. Phys. **56**, 287–295 (2003). https://doi.org/10.1016/s0360-3016(03)00087-7
5. Y. Yang, P.P. Zhang, L. Happersett et al., Choreographing couch and collimator in volumetric modulated arc therapy. Int. J. Radiat. Oncol. Biol. Phys. **80**, 1238–1247 (2011). https://doi.org/10.1016/j.ijrobp.2010.10.016
6. D. Nguyen, J. Rwigema, V. Yu et al., Feasibility of extreme dose escalation for glioblastoma multiforme using 4π radiotherapy. Radiat. Oncol. **41**, 264–265 (2014). https://doi.org/10.1016/j.ijrobp.2014.05.527
7. J.C.M. Rwigema, D. Nguyen, D. Heron et al., 4π noncoplanar stereotactic body radiation therapy for head-and-neck cancer: potential to improve tumor control and late toxicity. Int. J. Radiat. Oncol. Biol. Phys. **91**, 401–409 (2015). https://doi.org/10.1016/j.ijrobp.2014.09.043
8. E. Wilda, M. Bangert, S. Nill et al., Noncoplanar VMAT for nasopharyngeal tumors: Plan quality versus treatment time. Med. Phys. **42**(5), 2157–2168 (2015). https://doi.org/10.1118/1.4914863
9. P. Dong, P. Lee, D. Ruan et al., 4π noncoplanar stereotactic body radiation therapy for centrally located or larger lung tumors. Int. J. Radiat. Oncol. Biol. Phys. **86**, 407–413 (2013). https://doi.org/10.1016/j.ijrobp.2013.02.002
10. B. Fahimian, V. Yu, K. Horst et al., Trajectory modulated prone breast irradiation: a LINAC-based technique combining intensity modulated delivery and motion of the couch. Radiother. Oncol. **109**, 475–481 (2013). https://doi.org/10.1016/j.radonc.2013.10.031
11. P. Dong, D. Nguyen, D. Ruan et al., Feasibility of prostate robotic radiation therapy on conventional C-arm linacs. Pract. Radiat. Oncol. **4**, 254–260 (2014). https://doi.org/10.1016/j.prro.2013.10.009
12. A. Tran, J. Zhang, K. Woods et al., Treatment planning comparison of IMPT, VMAT and 4π radiotherapy for prostate cases. Radiat. Oncol. **12**, 10 (2017). https://doi.org/10.1186/s13014-016-0761-0
13. L. Rossi, S. Breedveld, B.J. Heijmen et al., On the beam direction search space in computerized non-coplanar beam angle

optimization for IMRT-prostate SBRT. Phy. in Med. & Biol. **57**, 5441–5458 (2012). https://doi.org/10.1088/0031-9155/57/17/5441
14. L. Rossi, S. Breedveld, S. Aluwini et al., Noncoplanar beam angle class solutions to replace time-consuming patient-specific beam angle optimization in robotic prostate stereotactic body radiation therapy. Int. J. Radiat. Oncol. Biol. Phys. **92**, 762–770 (2015). https://doi.org/10.1016/j.ijrobp.2015.03.013
15. V.Y. Yu, A. Tran, D. Nguyen et al., The development and verification of a highly accurate collision prediction model for automated noncoplanar plan delivery. Med. Phys. **42**, 6457–6467 (2015). https://doi.org/10.1118/1.4932631
16. T.D. Mann, N.P. Ploquin, W.R. Gill et al., Development and clinical implementation of eclipse scripting based automated patient-specific collision avoidance software. J. Appl. Clin. Med. Phys. **20**, 12–19 (2019). https://doi.org/10.1002/acm2.12673
17. S.J. Becker, Collision indicator charts for gantry-couch position combinations for Varian linacs. J. of Appl. Clin. Med. Phys. **12**, 3405–3411 (2011). https://doi.org/10.1120/jacmp.v12i3.3405
18. C. Hua, J. Chang, K. Yenice et al., A practical approach to prevent gantry-couch collision for linac-based radiosurgery. Med. Phys. **31**, 2128–2134 (2004). https://doi.org/10.1118/1.1764391
19. C.L. Ong, W.F. Verbakel, J.P. Cuijpers et al., Treatment of large stage I-II lung tumors using stereotactic body radiotherapy (SBRT): planning considerations and early toxicity. Radiother. Oncol. **97**, 431–436 (2010). https://doi.org/10.1016/j.radonc.2010.10.003
20. S. Derycke, B.V. Duyse, W.D. Gersem et al., Non-coplanar beam intensity modulation allows large dose escalation in stage III lung cancer. Radiother. Oncol. **45**, 253–261 (1997). https://doi.org/10.1016/S0167-8140(97)00132-1
21. J.Y.C. Cheung, K.N. Yu, Rotating and static sources for gamma knife radiosurgery systems: Monte Carlo studies. Med. Phys. **33**, 2500–2505 (2006). https://doi.org/10.1118/1.2207313
22. J.S. Kuo, C. Yu, Z. Petrovich et al., The CyberKnife stereotactic radiosurgery system: description, installation, and an initial evaluation of use and functionality. Neurosurgery. **53**, 785–789 (2003). https://doi.org/10.1227/01.neu.0000316282.07124.31
23. Y. Kamino, K. Takayama, M. Kokubo et al., Development of a four-dimensional image-guided radiotherapy system with a gimbaled X-ray head. Int. J. Radiat. Oncol. Biol. Phys. **66**, 271–278 (2006). https://doi.org/10.1016/j.ijrobp.2006.04.044
24. G.A. Weidlich, M.B. Schneider, J.R. Adler, Characterization of a novel revolving radiation collimator. Cureus **10**(2), e2146 (2018). https://doi.org/10.7759/cureus.2146
25. D. Papp, T. Bortfeld, J. Unkelbach, A modular approach to intensity-modulated arc therapy optimization with noncoplanar trajectories. Phys. Med. Biol. **60**, 5179–5198 (2015). https://doi.org/10.1088/0031-9155/60/13/5179
26. B. Wilson, K. Otto, E. Gete et al., A simple and robust trajectory-based stereotactic radiosurgery treatment. Med. Phys. **44**, 240–248 (2017). https://doi.org/10.1002/mp.12036
27. G. Smyth, P.M. Evans, J.C. Bamber et al., Non-coplanar trajectories to improve organ at risk sparing in volumetric modulated arc therapy for primary brain tumors. Radiother. Oncol. **121**, 124–131 (2016). https://doi.org/10.1016/j.radonc.2016.07.014